Wetting on structured substrates

2005 J. Phys.: Condens. Matter 17 S577

(http://iopscience.iop.org/0953-8984/17/9/017)

INSTITUTE OF PHYSICS PUBLISHING JOURNAL OF PHYSICS: CONDENSED MATTER

J. Phys.: Condens. Matter **17** (2005) S577–S593 doi:10.1088/0953-8984/17/9/017

Wetting on structured substrates

S Dietrich[1], **M N Popescu and M Rauscher**

Max-Planck-Institut für Metallforschung, Heisenbergstraße 3, 70569 Stuttgart, Germany
and
Institut für Theoretische und Angewandte Physik, Universität Stuttgart, Pfaffenwaldring 57, 70569 Stuttgart, Germany

E-mail: dietrich@mf.mpg.de, popescu@mf.mpg.de and rauscher@mf.mpg.de

Received 24 November 2004
Published 18 February 2005
Online at stacks.iop.org/JPhysCM/17/S577

Abstract

Chemically patterned surfaces are of significant interest in the context of microfluidic applications, and miniaturization of such devices aims at generating structures on the nano-scale. Whereas on the micron scale purely macroscopic descriptions of liquid flow are valid, on the nanometre scale long-ranged inter-molecular interactions, thermal fluctuations such as capillary waves, and finally the molecular structure of the liquid become important. We discuss the most important conceptual differences between flow on chemically patterned substrates on the micron scale and on the nanometre scale, and formulate four design issues for nanofluidics related to channel width, channel separation, and channel bending radius. As a specific example of nano-scale transport we present a microscopic model for the dynamics of spreading of monolayers on homogeneous substrates. Kinetic Monte Carlo simulations of this model on a homogeneous substrate reveal a complex spatio-temporal structure of the extracted monolayer, which includes the emergence of interfaces and of scaling properties of density profiles. These features are discussed and rationalized within the corresponding continuum limit derived from the microscopic dynamics. The corresponding spreading behaviour on a patterned substrate is briefly addressed.

1. Introduction

In recent years substantial efforts have been invested in miniaturizing chemical processes by building microfluidic systems. The 'lab on a chip concept' integrates a great variety of chemical and physical processes into a single device in a similar way as an integrated circuit incorporates many electronic devices into a single chip [1]. These microfluidic devices do not only allow for cheap mass production but they can operate with much smaller quantities

[1] Author to whom any correspondence should be addressed.

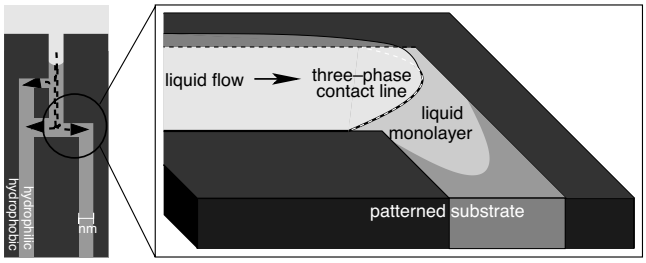

Figure 1. Schematic picture of liquid flow guided by so-called chemical walls on a chemically patterned substrate. The liquid moves along lyophilic stripes (light grey) on a lyophobic substrate (dark grey). The liquid layer ends in a three-phase contact line and a liquid monolayer (the precursor film) spreads ahead of it.

of reactants and reaction products than standard laboratory equipment. This is particularly important for rare and expensive substances such as certain biological substances and for toxic or explosive materials [2]. Even though most available microfluidic devices today have micron sized channels, further miniaturization is leading towards the nano-scale [2, 3]. Besides meeting technical challenges, new theoretical concepts are needed to understand the basic physical processes underlying this new technology [4, 5]. Whereas the ultimate limits for the miniaturization of electronic devices are set by quantum fluctuations, in a chemical chip these limits are determined by thermal fluctuations and can be explored by methods of classical statistical mechanics.

There are two main lines of development for microfluidic systems. The first one encompasses systems with closed channels. A common technique to produce these devices is to cast poly(dimethylsiloxane) (PDMS) over a topographically structured master, to peel off the polymer after curing, and to seal the resulting topographically structured material onto a flat surface. This way rather complicated devices including valves and pumps have been fabricated [6]. However, closed channel systems have the disadvantage that they can be easily clogged by solute particles such as colloids or large bio-polymers.

The second type of systems are open with a free liquid–vapour interface, and the fluid is not confined by physical but by chemical walls. The idea is that the liquid will be guided by lyophilic stripes on an otherwise lyophobic substrate. There are two sub-types of this technique: using a single chemically patterned substrate [7, 8] (see also figure 1) or a chemically patterned slit pore [5, 9, 10], respectively. The substrate surfaces can be structured chemically by printing or photographic techniques. All the techniques are confined to two dimensions.

Whereas the aforementioned examples deal with dynamic issues, there is also significant interest of basic and applied research in studying within thermal equilibrium liquids in contact with chemically or geometrically structured substrates [11]. Equilibrium wetting of chemically structured substrates has been studied extensively on all length scales [12–21]. For example, adsorption on stripe patterns shows a rich morphology on the macro-scale [18, 21] as well as on the nano-scale [11, 17] involving morphological phase-transitions. Recently, wetting of geometrically structured substrates has also received a lot of interest, with theoretical [22–24] and experimental [25, 26] studies revealing a filling transition below the wetting transition with a profound influence of the shape of the substrate on the adsorption isotherms [27–30]. In this context flow of liquids has also been studied to a large extent. Most of this research has been focused on homogeneous substrates, in particular on dynamic contact angles, dewetting of thin films, and flow of thin films (for a review see [31]). Recently, similar questions have been addressed for the case of patterned substrates [32–35].

At the sub-micron thickness scale, recent experiments on liquid spreading on atomically smooth surfaces [36–38], performed with volumes of the order of nano-litres, have clearly shown by means of dynamic ellipsometry or x-ray reflectivity measurements that a precursor film with one or a few layers with *molecular thickness* and *macroscopic extent* advance in front of the macroscopic liquid wedge of the spreading drop[2]. Theoretical work (see [40–42] and references therein) combined with an impressive number of molecular dynamics (MD) and Monte Carlo (MC) simulations (see [43] and references therein) addressed the mechanisms behind the extraction and the $t^{1/2}$ time dependence of the linear extent of the precursor films on homogeneous substrates [36, 40, 41]. This raises the issue of the lateral spatio-temporal structure of such monolayers [44] (see, cf, section 4). Based on the good understanding of the spreading dynamics and morphology on homogeneous substrates one can attack more complicated problems such as the spreading behaviour of monolayers exposed to chemical stripes or steps, junctions of chemical stripes, or mixing of different fluids.

In the following we briefly describe some equilibrium features of wetting on chemically patterned substrates which are most relevant for microfluidic applications (section 2.1). After discussing the characteristics of thin film flow on homogeneous substrates (section 2.2), we state three main conceptual differences between micro-scale and nano-scale fluid transport in chemical channels (section 3.1–3.3) and we formulate a number of design principles for nanofluidic devices (section 3.4). We then analyse the structure of monolayers spreading on homogeneous substrates (section 4) as a specific example of nano-scale transport.

2. Liquids on structured substrates

2.1. Wetting on chemically patterned substrates

Equilibrium wetting phenomena on chemically patterned substrates have been analysed theoretically in great detail on both the macroscopic and the microscopic scale. Microscopic theories, such as the successful density functional theory [45], take into account explicitly the finite range of inter-molecular attractions and short-ranged repulsions [11]. Density functional theories do not only allow one to study the order of wetting transitions and the equilibrium shape of the wetting film but also the detailed microscopic structure of the liquid in the vicinity of the substrate and at the liquid–vapour interface [4, 46].

In macroscopic theories, however, the inter-molecular interactions are approximated locally by using global quantities. For a wetting film this means that the free energy of the film is described by a bulk term proportional to the volume of the fluid, a surface tension term proportional to the area of the liquid–vapour interface, an interface term proportional to the area of the liquid–substrate interface, and a line tension term proportional to the length of the three-phase contact line between liquid, vapour, and substrate. In most studies the line tension term is neglected. Macroscopic theories have been used to describe the shape of droplets on homogeneous and structured substrates [18, 21]. The equilibrium droplet shape in chemically patterned slit-like pores has also been studied with the same technique [20].

It is a great challenge to describe the intermediate scale between the microscopic and the macroscopic one, in most cases it being impossible to obtain analytical results from microscopic theories while numerical simulations are prohibitive for large systems. Density functional theory has turned out to be a successful tool to address this intermediate scale [11]. In this context it has been possible to extend the scope of macroscopic theories down to the meso-scale by incorporating microscopic effects such as the wavelength dependence of the surface

[2] Thin (of the order of 100 nm) precursor films spreading ahead of the macroscopic droplet have been also experimentally observed [39].

tension [46] and detailed properties of the three-phase contact line such as its intrinsic structure, the magnitude of the line tension, and its temperature dependence [14, 47, 48].

2.2. Flow of thin liquid films

Flow of thin liquid films on homogeneous substrates has been studied extensively, in particular the motion of the three-phase contact line, dewetting of thin films, the stability of falling liquid films, and Marangoni flow. Apart from a few molecular dynamics simulations, in most studies the liquid flow is described in terms of meso-scale hydrodynamics. This means that the hydrodynamic equations are augmented with long-ranged liquid–substrate interactions and hydrodynamic slip of the liquid at the substrate (with slip lengths on the nanometre scale). For a review see [31]. In a phase-field description even compressibility effects and the finite width of the liquid–vapour interface have been taken into account [49]. Up to now, the finite interface width in the phase field models is the only signature of thermal fluctuations taken into account in hydrodynamic thin film models.

The main analytic tool in this approach is the so-called lubrication approximation, which is a small-gradient expansion for the film thickness and which leads to a fourth order in space, first order in time parabolic partial differential equation for the film thickness. This equation is also often referred to as the thin film equation and it has been successful in describing dewetting processes quantitatively [35]. Flow over chemical substrate inhomogeneities has been studied in the context of dewetting of unstable films [32], but to little extent for the actual situations relevant to microfluidics and nanofluidics [33, 34].

Recently the lubrication approximation has been extended to the situation of flow over a sharp chemical step. In this situation the lubrication approximation breaks down because in the vicinity of the chemical step the disjoining pressure varies laterally in the direction normal to the step on the same length scale as the film thickness. However, with asymptotic matching techniques, continuity conditions for the thin film equation on either side of the step have been derived. For equal values of the slip coefficient on either side of the chemical step the film thickness, the gradient of the film thickness, the reduced pressure, and the mass current are continuous [50].

3. Conceptual differences in microfluidics and nanofluidics

In this section we state three important conceptual differences between microfluidics and nanofluidics.

3.1. Triple line and chemical steps

One of the most critical issues in open microfluidic systems is to keep the liquid in the desired areas such as channels, reactors, and reservoirs. On a macroscopic scale the liquid will stay on the lyophilic channels for low filling, and the three-phase contact line will lie on the channel area or it will be pinned at the chemical step (see figure 2(a)). Spill-over onto the lyophobic areas occurs once the contact angle of the liquid at the chemical step exceeds the advancing contact angle α_a on the lyophobic area (which is in general larger than the equilibrium contact angle α_e due to surface defects), as shown in figure 2(b).

On the nano-scale the situation is quite different (see figures 2(c), (d)). First, the concepts of a contact line and contact angle have to be revised. A sharp contact line is replaced by a smooth transition from a mesoscopic wetting film to the precursor film [12, 13, 15, 17, 48] which is only a few molecular diameters thick and spreads ahead of the main portion of the

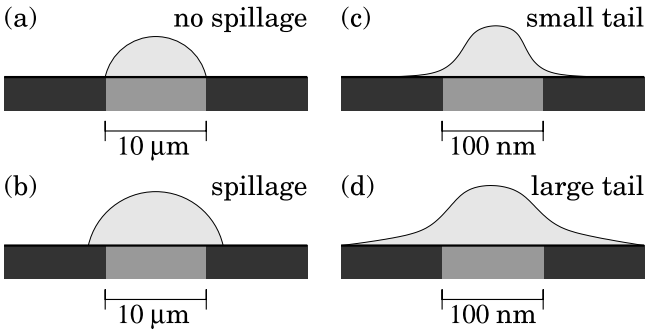

Figure 2. Spill-over of a liquid channel on a micron-sized chemical strip (left column) as compared to a nano-scale strip (right column). Dark grey marks the lyophobic areas and light grey the lyophilic areas. At the micron scale one can clearly distinguish between no spillage (a) and spillage (b), whereas for nano-channels one can only distinguish between small tails (c) and large tails (d) of the lateral liquid distribution.

moving liquid. Moreover, even an atomically sharp boundary between lyophilic and lyophobic areas on the substrate will lead to a smooth lateral variation of the interaction potential between the liquid particles and the substrate [12].

Thus the macroscopic and sharp criterion for a liquid staying on a chemical channel, namely whether the triple line crosses the channel boundary or not, becomes fuzzy at the nano-scale. Since there is always a certain amount of liquid on the lyophobic part of the substrate, one has to address the issue of which fraction of the liquid is outside the channels rather than whether there is liquid outside the channels.

3.2. Interaction between neighbouring channels

The question of spillage is of course closely related to the question of interaction between neighbouring channels. Macroscopically (neglecting evaporation and recondensation) two neighbouring channels will interact once the two liquid films merge. One has to keep in mind that in a macroscopic description an empty and a filled channel next to each other (figure 3(c)) or two filled but not interacting channels (figure 3(a)) can be metastable states. In the first case two equally filled channels and in the second case a liquid bridge can be the equilibrium state. How such configurations are affected by flow has not been investigated yet.

On the nano-scale, however, tails of the liquid from two neighbouring channels can leak onto the lyophobic area between the channels. If the channels are too close these tails will overlap and thus form a bridge (see figures 3(d)–(f)). Liquid can flow through such a bridge and particles immersed in the fluid can diffuse through these bridges. Thus keeping the two flows separated is a quantitative question of timescales and not a question that can be answered uniquely.

Also the presence of a monomolecular precursor film on the lyophobic area can lead to an exchange of molecules (see figure 3(f)). Macroscopically this is certainly negligible, but since the ratio between the film thickness in the channel and the thickness of the precursor film can be as small as 10, this can be significant at the nano-scale.

Fluctuations also become more important at small scales. In the absence of a precursor film on the area between the channels, a filled channel next to an empty one can be a metastable state as in the macroscopic case discussed above. But the energy barrier which has to be overcome to connect the two channels is much smaller than for macroscopic distances and much smaller fluctuations of the film height are sufficient for this process.

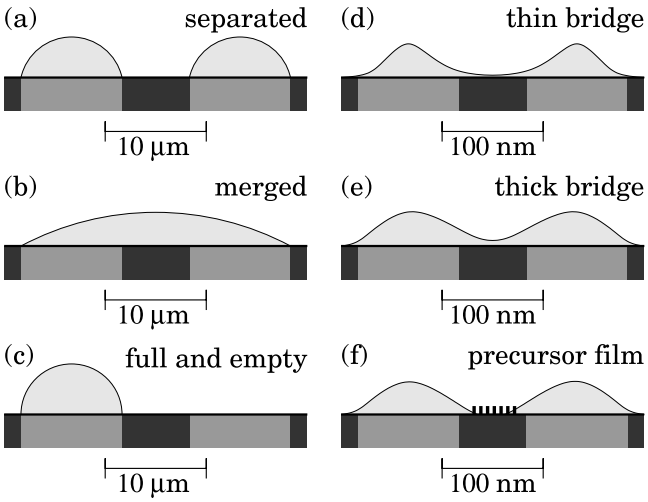

Figure 3. Interaction between neighbouring channels at the micron scale (left column) and at the nano-scale (right column). Dark grey marks the lyophobic areas and light grey the lyophilic areas. At the micron scale the flows are either well separated (a) or merged (b). Even a filled channel next to an empty one (c) is possible. At the nano-scale the tails of the liquid in the channels will merge and thus form a thin (d) or thick (e) bridge through which material can be interchanged. The thickness of the bridge is that of a monolayer in the case of a precursor film (f).

Not only do the liquid–substrate interactions have a range of up to 100 nm, but so does the liquid–liquid interaction. Thus within this range the direct interaction between liquid streams in parallel channels will influence the flow and also the thermal fluctuations.

3.3. Flow and the atomistic structure of liquids

The conclusions in the last two sections are mostly based on quasi-static considerations. Transport mechanisms and dynamic properties have not been discussed. Experience tells us that down to length scales of about 1–10 nm hydrodynamic theories provide a rather good description of liquid flow. However, even at the micron scale atomistic properties of the liquid show up via the slip length at the liquid–substrate interface and via the details of the regularization of the stress singularity at the moving triple line (see figure 4(a)).

In nanofluidic systems there is a window of length scales within which long-ranged intermolecular forces play a role and hydrodynamics is still applicable. This window is centred around film thicknesses of about 100 nm. Below this length scale the atomistic structure of the liquid comes into play. Currently only molecular dynamics simulations explore this atomic length scale region (see for example figure 4(b)).

3.4. Design issues for nanofluidics

For liquid flow inside chemically patterned micron-sized channels several design issues have been addressed [5]. Due to the conceptual differences between flow on the micron scale and flow on the nano-scale the answers given for the micron scale cannot be transferred directly to the nano-scale. However, the basic issues are similar: (1) How much liquid can a chemical channel contain before considerable spillage onto the lyophobic areas occurs? (2) How wide must the channels be to support flow? (3) How small can the radius of curvature of bends in

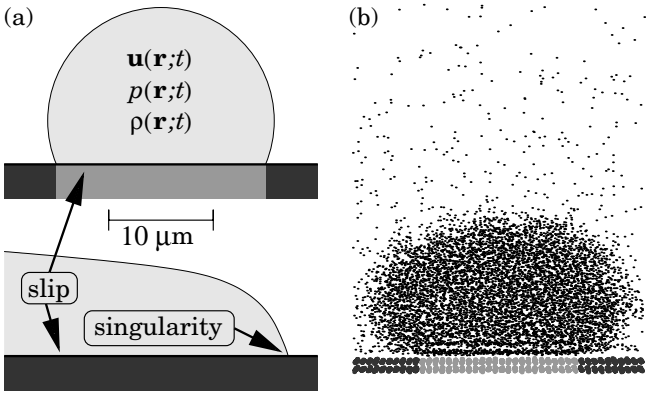

Figure 4. On the micron scale (a) (cross and longitudinal section) the flow can be described hydrodynamically, i.e., the liquid is described by the local flow field $\mathbf{u}(\mathbf{r};t)$, the local pressure $p(\mathbf{r};t)$, and the density $\rho(\mathbf{r};t)$. On the nano-scale (b) the atomic structure of the fluid and the substrate cannot be ignored [51].

the channel be? (4) What is the minimum distance between liquid streams below which they interact?

In micron scale channels these issues can be addressed by considering only surface tensions, contact angles, and line tensions. On the nano-scale the situation is more complex. In particular the details of the interaction between liquid and substrate, the interaction among the liquid molecules, the influence of the atomistic structure of the fluid on the transport properties, and thermal fluctuations have to be taken into account in addition.

4. Fluid monolayers on homogeneous substrates

It has been emphasized above that in the case of ultra-thin (monolayer) films the atomistic structure of the liquid and the details of the liquid–liquid and liquid–substrate interactions become dominant factors, and the dynamics of such films may be expected to be very different from that of flows at the micron scale [52]. Since at this small scale the liquid–substrate interaction is important, the flow of such ultra-thin (eventually monolayer) films may be controlled by engineering the physico-chemical properties of the substrate, thus opening the road for applications which do not have an equivalent at the macroscopic scale [5].

The dynamics of ultra-thin fluid films exposed to chemical steps can reveal a very complex behaviour, including, in the case of monolayers, the possibility of film rupture and strong density variations along and across the flow direction [44, 54]. As for the macroscopic situation, in order to elucidate the complex dynamics of ultra-thin films on structured substrates one has first to understand the details of the reference system, i.e., the dynamics and structure of a one-component fluid monolayer on a homogeneous substrate.

4.1. Model for spreading of fluid monolayers

In the following we briefly describe the defining rules of a simple microscopic model for the dynamics of a fluid monolayer in contact with a reservoir [53] based on the proposition in [41].

(a) We chose a rectangular (x–y plane) spreading geometry. The substrate is homogeneous. The half-plane $x < 0$ is occupied by a reservoir of particles (three-dimensional bulk

liquid) at fixed chemical potential which maintains at its contact line with the substrate, positioned at the line $x = 0$, an *average* density C_0 (defined as the number of particles per unit length in the transversal y direction). At time $t = 0$, the half-plane $x > 0$ is empty. For the case of capillary rise, the reservoir would correspond to the liquid bath and the line $x = 0$ to the edge of the macroscopic meniscus. There is no flow of particles from the reservoir to 'push' the film.

(b) The substrate–fluid interaction is modelled as a periodic potential forming a lattice of potential wells with coordination number z ($z = 4$ for a square lattice) and lattice constant a. The particle motion proceeds via activated jumps between nearest-neighbour wells; evaporation from the substrate is not allowed. The activation barrier U_A determines the jumping rate $\Omega = \nu_0 \exp[-U_A/k_B T]$, where ν_0 is an attempt frequency defining the time unit, k_B is the Boltzmann constant and T the temperature.

(c) The pair interaction between fluid particles at distance r is taken to be hard-core repulsive at short range, preventing double occupancy of the wells, and attractive at long range, $-U_0/r^6$ for $r \geqslant 1$, resembling a Lennard-Jones type interaction potential. The selection of the nearest-neighbour well, i.e., the probability $p(\boldsymbol{r} \to \boldsymbol{r}'; t)$ that a jump from location $\boldsymbol{r}$ will be directed toward the location $\boldsymbol{r}'$, is biased by the fluid–fluid energy landscape and is given by

$$p(\boldsymbol{r} \to \boldsymbol{r}'; t) = \frac{\exp\left\{\frac{\beta}{2}[\tilde{U}(\boldsymbol{r}; t) - \tilde{U}(\boldsymbol{r}'; t)]\right\}}{Z(\boldsymbol{r}; t)}, \tag{1}$$

where $Z(\boldsymbol{r}; t) = \sum_{\boldsymbol{r}', |\boldsymbol{r}'-\boldsymbol{r}|=1} \exp\{\frac{\beta}{2}[\tilde{U}(\boldsymbol{r}; t) - \tilde{U}(\boldsymbol{r}'; t)]\}$ is the normalization constant and $1/\beta = k_B T$,

$$\tilde{U}(\boldsymbol{r}; t) = -U_0 \sum_{\boldsymbol{r}', 0<|\boldsymbol{r}'-\boldsymbol{r}|\leqslant 3} \frac{\eta(\boldsymbol{r}'; t)}{|\boldsymbol{r} - \boldsymbol{r}'|^6}, \tag{2}$$

and $\eta(\boldsymbol{r}'; t) \in \{0, 1\}$ is the occupation number of the well at $\boldsymbol{r}'$ at the time t. The summation in equation (2) has been restricted to three lattice units for computational convenience. This corresponds to the cut-off generally used in molecular dynamics simulations for algebraically decaying Lennard-Jones pair-potentials. The rates

$$\omega_{\boldsymbol{r}\to\boldsymbol{r}';t} = \Omega p(\boldsymbol{r} \to \boldsymbol{r}'; t) \tag{3}$$

for the transitions from $\boldsymbol{r}$ to neighbouring locations $\boldsymbol{r}'$ satisfy

$$\sum_{\boldsymbol{r}', |\boldsymbol{r}'-\boldsymbol{r}|=1} \omega_{\boldsymbol{r}\to\boldsymbol{r}';t} \equiv \Omega. \tag{4}$$

Thus the total rate of leaving a location for any given particle at any given location is determined only by the fluid–solid interaction characterized by U_A, it is time independent, and it equals Ω.

(d) As defined by the rules (a)–(c), the model corresponds to mass transport from the reservoir into a two-dimensional vacuum so that a phase with very low density, due to two-dimensional evaporation, will form in front of the advancing monolayer. The emergence of this low-density phase poses problems in that its long time dynamics, which is of ideal gas type, mixes with that of the following-up 'compact' film and leads to serious difficulties in defining the advancing edge of the monolayer. In dealing with this problem we have adopted the following approach. We define the advancing edge Γ_t of a monolayer configuration at time t as the set of the most advanced particles in each line $y = const$ for this configuration. Two-dimensional 'evaporation' is eliminated by imposing an additional constraint: moves from sites $\boldsymbol{r} \in \Gamma_t$ toward sites $\boldsymbol{r}'$ ahead of Γ_t for which $|\tilde{U}(\boldsymbol{r}'; t)| < U_c$,

where $U_c \geqslant 0$ is a fixed threshold value, are rejected. This corresponds to requiring a given minimum number of particles in the neighbourhood $|\boldsymbol{r}| \leqslant r_c$ of any of the components of Γ_t. The results presented below correspond to simulations with $U_c = U_0/3^6$, i.e., $r_c = 3$; in other words to the requirement that in the disc $|\boldsymbol{r}'' - \boldsymbol{r}'| \leqslant 3$ centred at $\boldsymbol{r}'$ there is at least one more particle in addition to the one attempting the jump $\boldsymbol{r} \to \boldsymbol{r}'$. The above constraint is close in spirit to the 'effective boundary-tension' idea used in [41] in which the attractive interactions have been neglected except for particles on the advancing edge for which a *constant* asymmetry in the jumping rates 'away' and 'toward' the reservoir was imposed.

4.2. Kinetic Monte Carlo simulations results

We have carried out kinetic Monte Carlo (KMC) simulations of the model defined in the previous section [53] using a variable step continuous time kinetic Monte Carlo algorithm [55] and employing periodic boundary conditions along the transversal (y) direction (appropriate for simulating an infinitely wide substrate). In the simulations, the observables defined below have been measured.

The density $\rho(\boldsymbol{r}; t)$ is defined as $\rho(\boldsymbol{r}; t) = \langle \eta(\boldsymbol{r}; t) \rangle$, where $\langle \cdots \rangle$ means average over different KMC runs. Due to the symmetry of the model, the density profile $\tilde{\rho}(\boldsymbol{r}; t)$ in the limit of infinitely many runs is independent of y while, in the average over a finite number of runs, random uncorrelated fluctuations (whose amplitudes decrease with increasing number of runs) occur along the y direction. These fluctuations are suppressed by measuring the transversally averaged density $C(x, t) = \langle \frac{1}{L_y} \sum_{y=1}^{L_y} \eta(x, y; t) \rangle$, and thus it is expected that $C(x, t) \simeq \tilde{\rho}(\boldsymbol{r}; t)$, with strict equality for infinitely many runs. The average position of the advancing edge of the monolayer is defined as $X(t) = \langle \frac{1}{L_y} \sum_{\boldsymbol{r} \in \Gamma_t} x \rangle$. For the case $U_c = U_0/3^6$ (as used for the actual simulations), two-dimensional evaporation is negligible and $X(t)$ (which we shall also call the front line) is a good measure for the actual advancing edge of the monolayer. The activation energy was fixed to $\beta U_A = 3.5$.

We have studied the time dependence of the scaled front line, $X(t)/\sqrt{D_0 t}$ (where $D_0 = \Omega a^2/4$ is the one-particle diffusion coefficient on a bare substrate), for several values of the interaction parameter $W_0 = \beta U_0$ and of the reservoir density C_0.[3] Our results [53] show that at low and intermediate values of the interaction strength the previously reported $\sqrt{t}$ behaviour [36, 40, 41] is recovered independent of the value C_0 of the density in the reservoir. However, for strong attractive fluid–fluid interaction and low densities C_0, we have found that the time dependence of $X(t)$ clearly deviates from the $\sqrt{t}$ behaviour, the latter being obtained only for high densities C_0. Therefore, as a function of the interaction strength W_0 there is a transition from a 'substrate covering' state at low values W_0, in the sense of extraction of a film with macroscopic lateral extension in the spreading direction independently of the density value C_0 in the reservoir edge, i.e., a film which spreads according to $X(t \to \infty) \sim \sqrt{t}$, to a 'non-covering' state at large values W_0, in the sense that a macroscopic film is extracted only for sufficiently large densities C_0 (eventually for none if W_0 is sufficiently large).

For the 'substrate covering' state, from the curves $X(t)/\sqrt{D_0 t}$ one can estimate $A = \lim_{t \to \infty} X(t)/\sqrt{D_0 t}$ by fitting the data in the range $t \gg 1$ (in practice the data in the last tenth of the time interval available) with a constant, while for the 'non-covering' state we assume $A = 0$. The results for $A(C_0, W_0)$ are presented in figure 5 and they show that $A(C_0, W_0)$ is an increasing function of C_0 for fixed W_0 and a decreasing function of W_0 for fixed C_0. However,

[3] Here and in the following time t is measured in units of $\nu_0^{-1} = \Omega^{-1} \exp(-\beta U_A)$ with $\beta U_A = 3.5$, so that $\sqrt{D_0 t} = \sqrt{\nu_0 t} \frac{a}{2} \exp(-\frac{1}{2} \beta U_A)$.

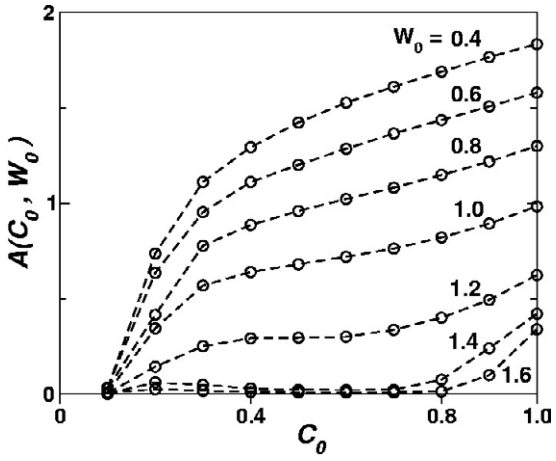

Figure 5. Dependence of the prefactor $A(C_0, W_0)$ on C_0 for several values of W_0. The symbols are KMC results; the dashed curves connecting the symbols are guides to the eye.

the functional dependence is not simple, and one can easily notice a change in the shape of $A(C_0, W_0)$ for W_0 close to the value 1.0. For values $W_0 \gtrsim 1$, the curve shows a plateau over a range of densities C_0 which increases with increasing W_0, while for values $W_0 \lesssim 1$ the prefactor A is a strictly increasing function of C_0. This change in behaviour emerges (see also the next section) as a consequence of the competition between the diffusive motion driven by the concentration gradient and the clustering tendency (opposing the concentration gradients) driven by the inter-particle attraction. From figure 5, the value of the threshold interaction $W_0^{(t)}$ for the onset of a plateau can be estimated to be bounded as $1.0 < W_0^{(t)} < 1.2$.

The KMC results in figure 5 indicate a threshold value $C_0^{(\min)} \simeq 0.1$ for the density in the reservoir edge below which, independent of the interaction strength W_0, there is no extraction of a monolayer: all the curves $A(C_0)$ reach zero at a non-zero value of C_0. This is a consequence of the condition (d) in the model, i.e., of the requirement that the density on an advancing edge should be at least $C_1 \simeq 0.1$ [53].

Since the time dependence of the advancing edge follows asymptotically $X(t) \sim \sqrt{t}$ in all the cases in which spreading occurs, it is natural to test if the density profiles $C(x, t)$ actually scale as a function of the scaling variable $\lambda = x/\sqrt{D_0 t}$. In figure 6 we show the density profiles $C(x, t)$ for (a) $W_0 = 1.0,\ C_0 = 1.0$ and (b) $W_0 = 1.4,\ C_0 = 1.0$ as functions of the scaling variable $\lambda = x/\sqrt{D_0 t}$. These results show that the density in the advancing monolayer depends significantly on the distance, and suggests that in the asymptotic limit ($t \gg 1$, $X(t) \gg 1$) the density profiles can be described by a scaling function $\tilde{C}(\lambda = x/\sqrt{D_0 t}; W_0, C_0)$ whose shape depends on the interaction strength W_0 and on the density C_0 at the edge of the reservoir.

As shown by the data in figure 6(b), for large W_0 the monolayer has an almost compact structure, and at the advancing edge there is a sharp transition from a large density to a small, almost zero, density. Therefore, in this case the spreading is accompanied by the emergence of a well defined interface between two phases. In contrast, at small W_0 the density decreases smoothly from the value at the edge of the reservoir to zero, and no jump in the density is visible (figure 6(a)). Thus $W_0^{(t)}$ is a threshold value above which the attractive interaction is strong enough to support the build-up of an interface, and the change at $W_0^{(t)}$ may be interpreted as the onset of a phase separation.

The formation of a 'foot' at the right end of the profile, of a height approximately equal to C_1 (e.g., in figure 6(a) at $\lambda \gtrsim 1.1$), is due to the fact that the density value on an *advancing*

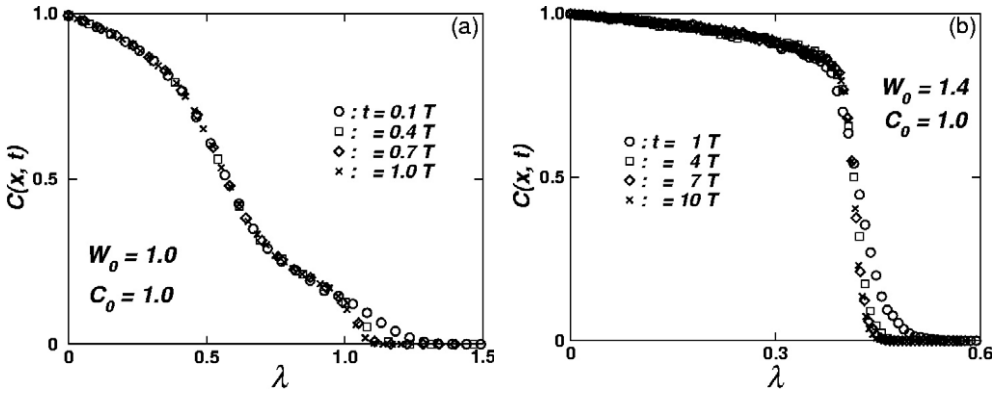

Figure 6. Density profiles $C(x,t)$ for (a) $W_0 = 1.0$, $C_0 = 1.0$ and (b) $W_0 = 1.4$, $C_0 = 1.0$ as functions of the scaling variable $\lambda = x/\sqrt{D_0 t}$.

edge Γ_t cannot decrease below C_1. This sharp interface occurs naturally due to the fact that the eventually large fluctuations are suppressed by blocking the advancing of isolated particles ahead of the film (see rule (d) in section 2), and thus the width of the interface would be expected to be of the order of the cut-off $r_c = 3$ of the attractive potential and to be almost constant in time. The height C_1 of the foot depends on the cut-off r_c of the attractive potential (increasing the value of r_c would lead to a smaller value C_1, and thus eventually to a hardly visible 'foot'), and in this sense it is a model-dependent feature.

4.3. Continuum limit

4.3.1. Differential equation for the density and scaling behaviour. Neglecting all spatial and temporal correlations, i.e., assuming that the averages of products of occupation numbers $\eta(\boldsymbol{r};t)$ are equal to the corresponding products of averaged occupation numbers $\rho(\boldsymbol{r};t) = \langle\eta(\boldsymbol{r};t)\rangle$, where $\langle\cdots\rangle$ denotes the average with respect to the corresponding probability distribution $\mathcal{P}(\{\eta(\boldsymbol{r};t)\})$ of a configuration $\{\eta(\boldsymbol{r};t)\}$, one can formulate a mean-field master equation for the local occupational probability (density) $\rho(\boldsymbol{r};t)$ [53]. In the continuum space and time limit ($\Delta t \to 0$, $a \to 0$, $\Omega^{-1} \to 0$, $D_0 = \Omega a^2/4$ finite) of the master equation, by taking Taylor expansions for $p(\boldsymbol{r} \to \boldsymbol{r}')$ and $\rho(\boldsymbol{r}';t)$ around $\boldsymbol{r}$ and keeping terms up to second-order spatial derivatives of the density $\rho(\boldsymbol{r};t)$ [53, 56], one obtains the following nonlinear and *nonlocal* equation for $\rho(\boldsymbol{r};t)$ [57, 58],

$$\partial_t \rho = D_0 \nabla\left[\nabla\rho + \beta\rho(1-\rho)\nabla U\right] + \mathcal{O}(a^2) \tag{5}$$

where

$$U(\boldsymbol{r};t) \equiv \langle\tilde{U}(\boldsymbol{r};t)\rangle = -U_0 \sum_{\boldsymbol{r}'',0<|\boldsymbol{r}''-\boldsymbol{r}|\leqslant 3} \frac{\rho(\boldsymbol{r}'';t)}{|\boldsymbol{r}''-\boldsymbol{r}|^6} \tag{6}$$

replaces $\tilde{U}(\boldsymbol{r};t)$ in the definition (1) for $p(\boldsymbol{r} \to \boldsymbol{r}')$.

The constraint of a fixed density C_0 at the edge $x = 0$ of the reservoir implies the boundary condition

$$\rho(x = 0, y; t) = C_0. \tag{7}$$

In the absence of formation of interfaces, i.e., for interactions $W_0 < W_0^{(t)}$, and for large times, the KMC results suggest that the density on the advancing edge $X(t)$ can be considered as

fixed and equal to C_1, leading to the boundary condition

$$\rho(x = X(t), y; t) = C_1. \tag{8}$$

In what follows, we shall use the value $C_1 = 0.11$ obtained in the KMC simulations[4].

Since there are no boundaries along the y-direction and the boundary conditions at $x = 0$ and $X(t)$ are independent of y, one has to solve an effectively one-dimensional problem; however, equation (5) remains quite complex because it is nonlocal due to the term involving the interaction potential $U(\boldsymbol{r}; t)$. Assuming that the density $\rho(\boldsymbol{r}; t)$ is a slowly varying function of the spatial coordinates (which certainly is a reasonable hypothesis everywhere except near interfaces; see figure 6), the potential $U(\boldsymbol{r}; t)$ may be expanded as

$$\begin{aligned} U(\boldsymbol{r}; t) &= -U_0 \sum_{\boldsymbol{r}', 0<|\boldsymbol{r}'-\boldsymbol{r}|\leqslant 3} \frac{\rho(\boldsymbol{r}'; t)}{|\boldsymbol{r}' - \boldsymbol{r}|^6} \\ &\simeq -U_0 \rho(\boldsymbol{r}; t) \sum_{\boldsymbol{r}', 0<|\boldsymbol{r}'-\boldsymbol{r}|\leqslant 3} \frac{1}{|\boldsymbol{r}' - \boldsymbol{r}|^6} + \mathcal{O}(a^2), \end{aligned} \tag{9}$$

which leads to the *local* equation

$$\partial_t \rho = D_0 \nabla\{[1 - g W_0 \rho(1 - \rho)] \nabla\rho\} + \mathcal{O}(a^2), \tag{10}$$

with $g = \sum_{1\leqslant|\boldsymbol{r}|\leqslant r_c} |\boldsymbol{r}|^{-6}$ a geometrical factor dependent on the lattice type (e.g., square, triangular, etc) and on the cut-off range of the potential. For the present case of a square lattice and a cut-off at $r_c = 3$ one has $g \simeq 4.64$.

Rescaling the time as $t \to \tau = D_0 t$ and defining an effective diffusion coefficient

$$D_e(\rho) = 1 - g W_0 \rho(1 - \rho), \tag{11}$$

equation (10) may be written in the usual form of a diffusion equation:

$$\partial_\tau \rho = \nabla [D_e(\rho) \nabla\rho] + \mathcal{O}(a^2). \tag{12}$$

The functional form of $D_e(\rho)$ (equation (11)) implies that for $W_0 > 4/g$ there will be values ρ_i of the density for which $D_e(\rho_i) < 0$. For parameters such that $W_0 < 4/g$, (12) is a proper diffusion equation, while for $W_0 > 4/g$ instabilities are expected in the range of densities where $D_e(\rho_i) < 0$, i.e., for $\rho_i \in \left(\rho_\alpha^-, \rho_\alpha^+\right)$ where

$$\rho_\alpha^\pm = \frac{1}{2}\left(1 \pm \sqrt{1 - \frac{4}{g W_0}}\right). \tag{13}$$

It is known [57, 59] that these instabilities are discontinuities in the density profile ('shocks'), i.e., they correspond to the formation of interfaces, as observed in the KMC results. Thus the value for the threshold interaction strength for which interfaces emerge is predicted by the continuum theory as $W_0^{(t)} = 4/g \simeq 0.86$, which is significantly smaller than the lower bound estimate $1.0 < W_0^{(t)}$ from KMC simulations. We attribute this to the mean-field character of the derivation of the continuum equation and look for a simple, intuitive way to include particle–particle correlations into the mean-field description. The dynamics is possible only by jumps into empty locations, which means that the summation in g should include at most three contributions from nearest-neighbour sites. This leads to $g \simeq 3.64$ and an estimate for the threshold interaction $W_0^{(t)} \simeq 1.1$, in good agreement with the KMC results. For the rest of the analysis we will use this corrected value of g.

[4] The boundary condition equation (8) naturally occurred also in the theory of Burlatsky *et al* [62].

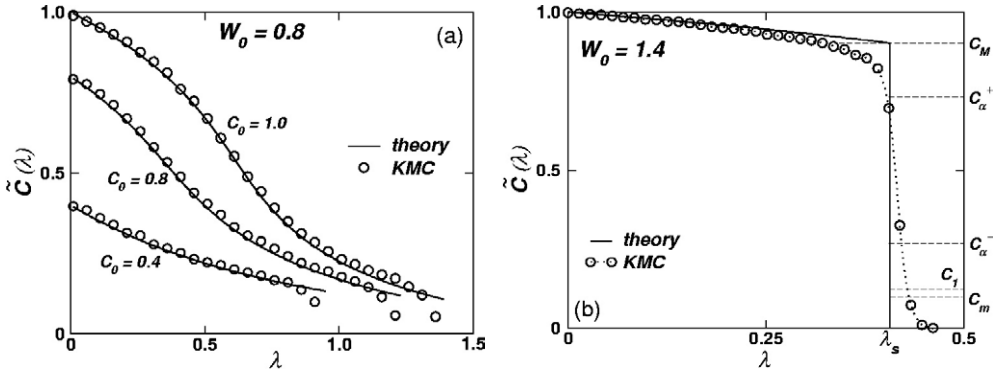

Figure 7. (a) Asymptotic scaling solution $\tilde{C}(\lambda)$ for $W_0 = 1.0$, $\tilde{C}(\lambda = 0) = C_0 = 1.0, 0.8, 0.4$ with $\lambda = x/\sqrt{D_0 t}$. Shown are theoretical results from (14) (solid curves) and corresponding KMC results at time $T = 2 \times 10^6$ (open circles) (assumed to be close to the asymptotic limit). (b) Asymptotic scaling solution $\tilde{C}(\lambda)$ for $W_0 = 1.4$, $C_0 = 1.0$. Shown are theoretical results obtained from equations (14), (17), and (19) (solid curves), and corresponding KMC results at time $T = 2 \times 10^7$ (open circles) (assumed to be close to the asymptotic limit). The dotted curve is a guide to the eye. The dashed lines indicate the corresponding values C_m and C_M from 18, $C_\alpha^\pm$ from 13 where $D_e(C_\alpha^\pm) = 0$, which determines the onset of the density range leading to instabilities, C_1 from the boundary condition (15*b*), and the position λ_s of the discontinuity given by (19).

Since the solution of equation (12) depends only on x, after introducing the scaling variable $\lambda = x/\sqrt{\tau}$ one obtains the equation satisfied by the scaling solution $\tilde{C}(\lambda)$ in the asymptotic limit $t \gg 1$

$$\frac{\lambda}{2}\frac{d\tilde{C}}{d\lambda} + \frac{d}{d\lambda}\left[D_e(\tilde{C})\frac{d\tilde{C}}{d\lambda}\right] + \mathcal{O}[(a/\sqrt{\tau})^2] = 0 \tag{14}$$

with the boundary conditions

$$\tilde{C}(0) = C_0, \tag{15a}$$

$$\tilde{C}(A) = C_1. \tag{15b}$$

The solution of equation (14) depends on whether $W_0 < W_0^{(t)}$ or $W_0 > W_0^{(t)}$, and we shall discuss these two cases separately.

4.3.2. Scaling solutions. For $W_0 < W_0^{(t)}$, in equation (14) the term $\mathcal{O}[(a/\sqrt{\tau})^2]$ may be neglected and (14) together with the boundary conditions given in equation (15*a*) admits a regular solution $\tilde{C}(\lambda; W_0, C_0)$. This cannot be found in closed form, but the numerical integration of equation (14) is straightforward. Typical results for small and intermediate values of the attractive coupling W_0 are presented in figure 7(a) for several values of C_0.

There is excellent agreement in all cases between the theoretical results from (14) and the KMC results. Similar conclusions hold for all values of C_0 and $W_0 \leqslant 1.0$ [53]. In particular, the formation of a 'shoulder' in the case in which W_0 is large (see in figure 7(a) the curve corresponding to $C_0 = 1$) is remarkably well reproduced by the theoretical curve obtained from equation (14) [53]. Therefore we conclude that, even below the threshold value $W_0^{(t)}$ for interface formation, the inter-particle attraction has to be explicitly included in the model in order to obtain a correct prediction for the mass distribution inside the monolayer which is extracted.

In the case $W_0 > W_0^{(t)}$, the effective diffusion coefficient $D_e(\tilde{C})$ becomes negative within a range of densities and this leads to discontinuities ('shocks') in the solution $\tilde{C}(\lambda)$ in the long-

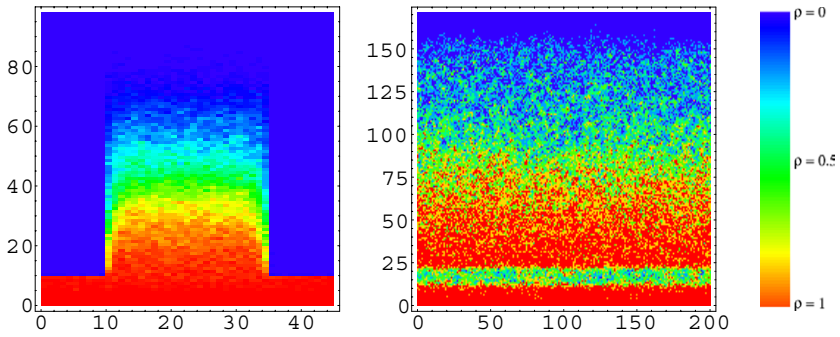

Figure 8. Examples of two-dimensional density profiles $\rho(x, y; t)$ at long time (obtained by averaging over 20 KMC runs) for spreading along a high affinity stripe located at $10 \leqslant y \leqslant 35$, $x > 10$ (left) or hitting a low affinity stripe located at $15 \leqslant y \leqslant 25$ (right). The colour coding (shown on the right) is a linear function of density.

time limit if the small terms $\mathcal{O}[(a/\sqrt{\tau})^2]$ (see equation (14)) are set to zero [59]. The existence and uniqueness of a 'weak' solution $\tilde{C}(\lambda)$ ('weak' in the sense that $\tilde{C}(\lambda)$ has a discontinuity at a point $\lambda = \lambda_s$ but satisfies (14) for $\lambda \neq \lambda_s$) have been recently addressed by Witelski [60, 61] using singular perturbation methods. We will use here directly the explicit construction of the shock solution (for more details see [53]).

We look for a weak solution of equation (14), subject to the boundary conditions given in (15*a*), in the form of a 'shock' defined as [60, 61]

$$\tilde{C}(\lambda) = \begin{cases} C_\ell(\lambda), & \lambda < \lambda_s, \\ C_r(\lambda), & \lambda > \lambda_s, \end{cases} \tag{16}$$

where $C_\ell(\lambda)$ and $C_r(\lambda)$ satisfy (14) in the intervals $[0, \lambda_s)$ and $(\lambda_s, A = X(t)/\sqrt{\tau}]$, respectively, subject to the boundary conditions

$$\begin{aligned} &C_\ell(0) = C_0, \qquad C_\ell(\lambda_s) = C_M, \\ &C_r(\lambda_s) = C_m < C_M, \qquad C_r(A) = C_1, \end{aligned} \tag{17}$$

respectively.

The values C_M and C_m of the density at the left and the right of the shock, respectively, are determined using a singular perturbation analysis of equation (14),

$$C_{M,m} = \frac{1}{2} \pm \frac{\sqrt{3}}{2}\sqrt{1 - \frac{4}{gW_0}}, \tag{18}$$

and the position λ_s of the shock is given by[5]

$$\lambda_s = -2\left[D_e(C_M)\left.\frac{dC}{d\lambda}\right|_{C_M} - D_e(C_m)\left.\frac{dC}{d\lambda}\right|_{C_m}\right] \Big/ (C_M - C_m). \tag{19}$$

Since the system of equations (14), (17), and (19) cannot be solved in closed form for the shock solution, we have solved it numerically. Such a numerical solution is shown in figure 7(b) for $W_0 = 1.4$ and $C_0 = 1.0$, for which $C_m \simeq 0.098 \lesssim C_1$. It can be seen that the agreement between the theoretical asymptotic 'shock' solution and the KMC measured

[5] For sufficiently large values W_0 of the attractive interaction the density C_m may become smaller than C_1 [53]. Since the density at the advancing edge cannot be smaller than C_1, in this case the branch $C_r(\lambda)$ disappears and the shock position is obtained by setting $C_m = 0$ in (19).

density profile is good. The KMC results confirm the value C_M as the onset of large density gradients, and there is good agreement between the theoretical prediction and the simulations in the range of densities $C > C_M$. The discrepancies in the range $C < C_M$ are probably due to too short simulations times.

The jump $C_M - C_m$ in the density at λ_s explains the formation of the plateau (for $W_0 > W_0^{(t)}$) in the dependence of $A(C_0, W_0)$ on C_0: if the density C_0 at the reservoir is within the range $C_m \leqslant C_0 < C_M$, in the immediate vicinity of the reservoir edge the density drops to C_m and in the long-time limit the extraction of the film proceeds effectively as if the reservoir density would have been C_m. Also, since $1/2 - C_m = -1/2 + C_M$, it follows that the plateau should be symmetric with respect to $C_0 = 0.5$; indeed the KMC data in figure 5 exhibit this symmetry (as long as W_0 is such that $C_m > 0.1$). Moreover, since the density must satisfy $C \leqslant 1$, one may conclude that for interaction values W_0 such that $C_M > 1$ the extraction of a monolayer is no longer possible. This implies that the exact value for the upper limit of the interaction $\widetilde{W}_0^{(\mathrm{cov})}$ above which no macroscopic film is extracted from the reservoir is given by $\widetilde{W}_0^{(\mathrm{cov})} = 6/g \simeq 1.65$.

4.4. Outlook to monolayers on patterned substrates

As a simple example of spreading on heterogeneous substrates we have used the same model to investigate the case of monolayers exposed to chemical patterns in the form of longitudinal (along the x-direction) stripes of high affinity on a low affinity substrate or transversal (along the y-direction) low affinity stripes on a high affinity substrate [54]. At the border between the high and low affinity domains we have assumed an energy barrier ΔU which acts against the motion from high to low affinity regions [44, 54]. Examples of spreading in such geometries are shown in figure 8. It can be seen that the density profiles become very complex, with variations along both longitudinal and transversal directions in the case of longitudinal stripes or with sharp interior interfaces in the case of transversal stripes. A continuum limit description of such problems will be presented elsewhere [54].

5. Summary and discussion

In this work we have discussed some of the important issues in wetting on structured substrates in the context of the miniaturization of microfluidic devices towards the nano-scale. Whereas on the micron scale purely macroscopic descriptions of liquid flow are valid, on the nanometre scale long-ranged inter-molecular interactions, thermal fluctuations such as capillary waves, and finally the molecular structure of the liquid become important.

Recent results on equilibrium wetting on patterned substrates and on flow on homogeneous substrates have been addressed in sections 2.1 and 2.2, respectively.

Section 3 has been devoted to a detailed discussion of the most important conceptual differences between flow on chemically patterned substrates on the micron scale and on the nanometre scale. We explained how the (macroscopic) question of the triple line crossing the channel boundary or not is replaced at the nano-scale by that of the fraction of the liquid outside the channels (figure 2), and how this transforms the (macroscopic) qualitative issue of separated flows in neighbouring channels into a quantitative question of space-time scales (figure 3). The closely related issue of the atomistic structure of the liquid (figure 4) when the relevant length scale is below 100 nm was briefly addressed in section 3.3. This discussion has led to the formulation of four design issues for nanofluidics (related to channel width, separation, and bending radius) listed in section 3.4.

As a specific example of nano-scale transport in section 4 we have discussed the spreading of fluid monolayers extracted from reservoirs. We have presented a microscopic lattice-gas

model with interacting particles, and have studied it using kinetic Monte Carlo simulations and a nonlinear diffusion equation within the continuum limit. The two-dimensional KMC simulations confirm the time dependence $X(t \to \infty) = A\sqrt{t}$ of the spreading, where $X(t)$ is the average position of the advancing edge of the monolayer at time t, and reveal a non-trivial dependence of the prefactor A on the strength W_0 of inter-particle attraction and on the fluid density C_0 at the reservoir (figure 5). The asymptotic (i.e., at long time and large spatial scales) transversally averaged density profiles $C(x, t)$ measured in the KMC simulations exhibit a scaling behaviour as function of the scaling variable $\lambda = x/\sqrt{D_0 t}$, where D_0 is the one-particle diffusion coefficient on the bare substrate (figure 6), and reveal the formation of sharp interfaces inside the extracted monolayer for strong interparticle attraction. These asymptotic, scaled density profiles have been analysed within a continuum limit with the corresponding nonlinear diffusion equation in which we have included the effect of correlations in an effective manner by adapting the value of the integrated attractive interaction to account for the presence of empty nearest-neighbour sites (figure 6). The formation of the interfaces in the range $W_0 > W_0^{(t)}$ has been related to instabilities of the diffusion equation associated with densities for which the corresponding effective diffusion coefficient becomes negative, and the analysis allowed us to predict $W_0^{(t)} = 1.1$ in good agreement with the KMC results. A singular perturbation analysis led us to the estimate $\widetilde{W}_0^{(\mathrm{cov})} \simeq 1.65$ as the threshold interparticle interaction, above which no macroscopic film is extracted from the reservoir. Finally, we briefly addressed the complex behaviour of spreading monolayers on structured substrates and presented two-dimensional density profiles (figure 8) which are typical for this case.

References

[1] Giordano N and Cheng J-T 2001 *J. Phys.: Condens. Matter* **13** R271
[2] Mitchell P 2001 *Nat. Biotech.* **19** 717
[3] Stone H A and Kim S 2001 *AIChE J.* **47** 1250
[4] Dietrich S 1998 *J. Phys.: Condens. Matter* **10** 11469
[5] Zhao B, Moore J S and Beebe D J 2002 *Anal. Chem.* **74** 4259
[6] Jeon N L *et al* 2002 *Biomed. Microdev.* **4** 117
[7] Gau H, Herminghaus S, Lenz P and Lipowsky R 1999 *Science* **283** 46
[8] Darhuber A A, Troian S M and Reisner W W 2001 *Phys. Rev.* E **64** 031603
[9] Handique K, Burke D T, Mastrangelo C H and Burns M A 2000 *Anal. Chem.* **72** 4100
[10] Lam P, Wynne K J and Wnek G E 2002 *Langmuir* **18** 948
[11] Dietrich S 1999 *New Approaches to Old and New Problems in Liquid State Theory* (*NATO-ASI Series C* vol C529) ed C Caccamo *et al* (Dordrecht: Kluwer) pp 197–244
[12] Koch W, Dietrich S and Napiórkowski M 1995 *Phys. Rev.* E **51** 3300
[13] Bauer C and Dietrich S 1999 *Phys. Rev.* E **60** 6919
[14] Bauer C and Dietrich S 1999 *Eur. J. Phys.* B **10** 767
[15] Bauer C, Dietrich S and Parry A O 1999 *Europhys. Lett.* **47** 474
[16] Bauer C 1999 Benetzung chemisch strukturierter Substrate *PhD Thesis* Bergische Universität-Gesamthochschule Wuppertal
[17] Bauer C and Dietrich S 2000 *Phys. Rev.* E **61** 1664
[18] Lenz P and Lipowsky R 2000 *Eur. Phys. J.* E **1** 249
[19] Rascon C and Parry A O 2001 *J. Chem. Phys.* **115** 5258
[20] Valencia A, Brinkmann M and Lipowsky R 2001 *Langmuir* **17** 3390
[21] Brinkmann M and Lipowsky R 2002 *J. Appl. Phys.* **92** 4296
[22] Rejmer K, Dietrich S and Napiórkowski M 1999 *Phys. Rev.* E **60** 4027
[23] Milchev A, Müler M, Binder K and Landau D P 2003 *Phys. Rev. Lett.* **90** 136101
[24] Milchev A, Müler M, Binder K and Landau D P 2003 *Phys. Rev.* E **68** 031601
[25] Bruschi L, Carlin A and Mistura G 2000 *J. Chem. Phys.* **115** 6200
[26] Bruschi L, Carlin A and Mistura G 2002 *Phys. Rev. Lett.* **89** 166101
[27] Rascon C and Parry A O 2000 *Nature* **407** 986

[28] Rascon C and Parry A O 2000 *J. Chem. Phys.* **112** 5175
[29] Parry A O, Macdonald E D and Rascon C 2001 *J. Phys.: Condens. Matter* **13** 383
[30] Bruschi L, Carlin A, Parry A O and Mistura G 2003 *Phys. Rev.* E **68** 021606
[31] Oron A, Davis S H and Bankoff S G 1997 *Rev. Mod. Phys.* **69** 931
[32] Kargupta K and Sharma A 2001 *Phys. Rev. Lett.* **86** 4536
[33] Kondic L and Diez J A 2002 *Phys. Rev.* E **65** 045301
[34] Brusch L, Kühne H, Thiele U and Bär M 2002 *Phys. Rev.* E **66** 011602
[35] Becker J *et al* 2003 *Nat. Mater.* **2** 59
[36] Heslot F, Cazabat A M, Levinson P and Fraysse N 1990 *Phys. Rev. Lett.* **65** 599
[37] Albrecht U, Otto A and Leiderer P 1992 *Phys. Rev. Lett.* **68** 3192
[38] Voué M, Valignat M P, Oshanin G, Cazabat A M and De Coninck J 1998 *Langmuir* **14** 5951
[39] Kavehpour H P, Ovryn B and McKinley G H 2003 *Phys. Rev. Lett.* **91** 196104
[40] de Gennes P G and Cazabat A M 1990 *C. R. Acad. Sci.* II **310** 1601
[41] Oshanin G G, De Coninck J, Cazabat A M and Moreau M 1998 *J. Mol. Liquids* **76** 195
[42] Abraham D B, Cuerno R and Moro E 2002 *Phys. Rev. Lett.* **88** 206101
[43] De Coninck J 1996 *Colloids Surf.* A **114** 155
[44] Popescu M N and Dietrich S 2003 *Interface and Transport Dynamics* ed H Emmerich, B Nestler and M Schreckenberg (Heidelberg: Springer) pp 202–7
[45] Evans R 1990 *Liquids at Interfaces* (*Les Houches Session XLVIII*) ed J Charvolin, J F Joanny and J Zinn-Justin (Amsterdam: Elsevier) pp 1–98
[46] Mecke K R and Dietrich S 1999 *Phys. Rev.* E **59** 6766
[47] Indekeu J O 1994 *Int. J. Mod. Phys.* B **8** 309 and references therein
[48] Getta T and Dietrich S 1998 *Phys. Rev.* E **57** 655
[49] Pismen L M 2002 *Colloids Surf.* A **206** 11
[50] Rauscher M 2003 unpublished
[51] Koplik J, unpublished
[52] Voué M and De Coninck J 2000 *Acta Mater.* **48** 4405
[53] Popescu M N and Dietrich S 2004 *Phys. Rev.* E **69** 061602
[54] Popescu M N and Dietrich S, unpublished
[55] Adam E, Billard L and Lançon F 1999 *Phys. Rev.* E **59** 1212
[56] Leung K-t 2000 *Phys. Rev.* E **63** 016102
[57] Giacomin G and Lebowitz J L 1996 *Phys. Rev. Lett.* **76** 1094
[58] Vlachos D G and Katsoulakis M A 2000 *Phys. Rev. Lett.* **85** 3898
[59] Elliott C M and French D A 1987 *IMA J. Appl. Math.* **38** 97
[60] Witelski T P 1995 *Appl. Math. Lett.* **8** 27
[61] Witelski T P 1996 *Stud. Appl. Math.* **96** 277
[62] Burlatsky S F, Oshanin G, Cazabat A M and Moreau M 1996 *Phys. Rev. Lett.* **76** 86